Available online at www.sciencedirect.com

SciVerse ScienceDirect

Ceramics International 39 (2013) 1021–1027

CERAMICS INTERNATIONAL

www.elsevier.com/locate/ceramint

Effect of annealing and room temperature sputtering power on optoelectronic properties of pure and Al-doped ZnO thin films

D. Podobinski[a], S. Zanin[a], A. Pruna[a,b,*,1], D. Pullini[a]

[a]*Centro Ricerche Fiat S.C.p.A., Strada Torino 50, 10043 Orbassano, Italy*
[b]*University Politehnica of Bucharest, 010737 Bucharest, Romania*

Received 11 June 2012; received in revised form 3 July 2012; accepted 4 July 2012
Available online 17 July 2012

Abstract

Transparent ZnO and Al-doped ZnO (AZO) thin films have been prepared by radio frequency sputtering deposition at room temperature. The optical, electrical, and structural characteristics of the obtained films have been extensively investigated as a function of sputtering and annealing parameters. Spectrophotometry, X-ray diffraction (XRD), atomic force microscopy (AFM), four-point probe and Hall-effect measurements were employed. The ZnO films generally exhibited excellent crystalline properties, while providing a UV cut-off in the absorption spectrum for optical filtration. AZO thin films exhibited an average transparency (larger than 85%) over the visible region of the spectrum, and resistivity of the order of $10^{-3}\,\Omega$ cm was obtained. The carrier concentration and electron mobility values proved to be dependent on the deposition parameters and annealing temperature. The obtained results showed that annealing temperatures higher than 400 °C were not necessary and potentially degraded the electronic properties of the AZO thin films.

Keywords: A. Films; C. Electrical properties; C. Optical properties; D. ZnO

1. Introduction

Transparent conductive oxides (TCOs) continue to be at the forefront of semiconductor research due to their appealing electronic and optical properties such as high conductivities and transparencies within the visible and IR region of the spectrum. Indium Tin Oxide (ITO) is one of the most largely used TCO's in industry, specifically for photovoltaics [1], LED [2] and OLED devices [3]. However, due to the increasing cost of indium, alternatives are being explored.

Zinc Oxide (ZnO) thin films began to attract research interest the early 1970s and its properties were explored for their potential in optoelectronic devices [4–6]. Interesting aspects of ZnO include: the anisotropy in crystal structure, wide band gap, the optical transparency in visible range, fairly high refractive index and large piezoelectric constant, respectively.

Undoped ZnO usually presents a high resistivity due to a low carrier concentration [7] and regardless the deposition method it has unstable electric properties in the long term. This instability of the undoped ZnO was related to the change in surface conductance under oxygen chemisorptions and desorption. However, it is known that conductive properties of ZnO depend on its stoichiometry and presence of impurities (dopants). N-type doping has been achieved by the substitution of Zn with group-III elements such as Al, Ga, In or by substitution of oxygen with group-VII elements such as Cl or I [8–12]. Aluminum-doped ZnO (AZO) provides attractive alternative to ITO [13,14]. Even if AZO conductivity still does not surpass the ITO one, it is considered for manufacturing transparent electrodes in flat panel displays, solar cells and organic light-emitting diodes due to their high electro-optical quality, high material availability and low material cost for large area applications [15–19] and its chemical stability in specific environment such

*Corresponding author. Tel.: +0034 627018518.
E-mail addresses: apruna@itm.upv.es, ai.pruna@gmail.com (A. Pruna).
[1]Present address: Institute of Materials Technology, University Politécnica of Valencia, Camino de Vera s/n 46022, Valencia, Spain.

0272-8842/$36.00
http://dx.doi.org/10.1016/j.ceramint.2012.07.022

as the hydrogen environment typical for thin-film Si solar cells, as well.

AZO films have been deposited using a multitude of methods, including spray pyrolysis [20], electrodeposition [21], sol–gel [22] and direct current (DC)/radio frequency (RF) sputtering [13]. Among these deposition processes, magnetron sputtering is considered to be a suitable technique due to its inherent characteristics such as high deposition rate, good controllability and scalability to large areas [23]. AZO layers prepared at room temperature or higher followed by subsequent annealing treatment at a higher temperature presented different properties as a function of the annealing atmosphere [24]. In order to achieve a better understanding of the influence of the sputtering power and annealing temperature on such film properties, higher knowledge of the interrelation between the structural, electrical and optical characteristics of AZO films is essential.

In this work, AZO thin films have been deposited by sputtering at room temperature and subsequently annealed in an inert atmosphere. Their structural, optical and electrical properties were analyzed as a function of sputtering power and annealing temperature and further compared to the ZnO ones deposited in the same conditions.

A better understanding of the dependence on the deposition conditions of different characteristics of the AZO films is aimed in this work. This will contribute to optimize the optoelectronic quality of the material as transparent and conductive electrode.

2. Experimental

2.1. Materials

Depositions were performed employing 2 in. diameter ZnO (99.99% purity) and AZO (2% Al_2O_3 concentration, 99.99% purity) sputtering targets (K. J. Lesker). Prior to sputtering, glass substrates (Schott AF-45 borosilicate) were prepared by ultrasonically cleaning in dilute detergent solution and subsequent rinsing with distilled water, acetone and isopropanol for 10 min each and followed by drying under nitrogen.

2.2. Synthesis

High purity Ar gas (99.99%) was introduced after the vacuum chamber was evacuated at 1×10^{-5} Torr. The process total pressure values were kept constant at 50 mTorr and 30 mTorr for ZnO and AZO, respectively. The substrate ($3 \times 3\ cm^2$) was placed parallel to the sputtering target and the target-substrate distance was always maintained constant at 9 cm while the sputtering power was varied in the range 70 W–160 W and the corresponding power densities ranged 3.45–7.89 W cm^{-2}. For practical application of the ZnO and AZO thin films, the obtained film thickness was kept at 200 nm. Upon deposition, annealing treatment of the thin films was performed in an Ulvac-Riko Mika-5000 chamber subjected to low pressure Ar atmospehere at 1×10^{-2} Torr as follows: 1 h at 400 °C for ZnO films and 1 h at 400, 500 and 600 °C for AZO ones.

2.3. Characterization methods

The film thickness was measured using a Tencor P-10 profilometer. A Cary 500 spectrophotometer (Varian) was employed for the optical characterization in the typical 300–800 nm wavelength range. Film topography was studied by atomic force miscroscopy (AFM) using a Veeco 3100 microscope. X-ray diffraction (XRD) measurements were performed using a SEIFERT 3003 PTS equipment with CuK_α radiation ($\lambda = 1.5405$ Å). Four-point probe technique was employed for the conductivity measurements and mobility measurements were taken using the Van der Pauw method.

3. Results and discussion

3.1. Structural properties

The XRD measurements revealed that all of the ZnO films obtained at room temperature were polycrystalline with the hexagonal structure and had a preferred orientation with the *c*-axis perpendicular to the substrate. Fig. 1 depicts some

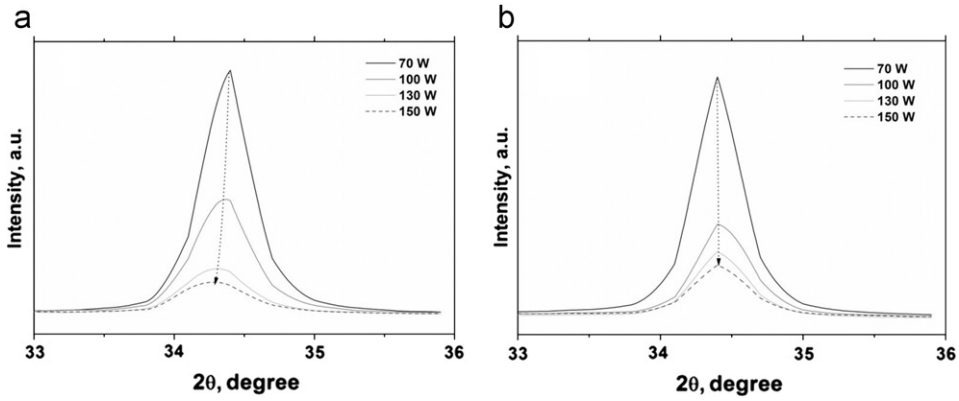

Fig. 1. XRD diffractograms corresponding to (a) as-prepared and (b) annealed ZnO films.

of the XRD diffractograms obtained for ZnO films as a function of sputtering power before and after annealing treatment. All the films were dominated by the (002) texture, with the diffraction peak located at $2\theta = 34.5/34.7^{\circ}$. To better evidence the effect of the varying parameter on the (002) peak, only the corresponding 2θ range is depicted. The lattice parameters were calculated using the formula

$$d_{hkl} = \left[4\left(h^2+k^2+hk\right)/3a^2 + l^2/c^2\right]^{-1/2} \quad (1)$$

where a and c represent the lattice parameters and d_{hkl} is the crystalline surface distance for h k l indices. The obtained value ranging 5.209–5.234 Å was close to the known Joint Committee on Powder Diffraction Standard (JCPDS) value ($c = 5.205$ Å). The intensity and the width at half maximum of the diffraction peak were found to be dependent on the sputtering power and the heating treatment, indicating changes in the mean crystallite size for the different samples. As it can be observed in Fig. 1a, the (002) diffraction angle is slightly shifted to the smaller 2θ upon increasing the sputtering power, indicating a slight crystal lattice deformation resulting from stress in the films. Generally, the intensities of the diffraction peaks decreased with increasing sputtering power due to the modified crystallinity of the resulting films and crystallite sizes becoming smaller (see Fig. 2). After the annealing treatment, the XRD peaks were located at the same 2θ value, with the corresponding c axis value ($c = 5.2055$ Å) very close to the JCPDS one, as shown in Fig. 1b. Such a change is expected if the Zn:O ratio within the crystal is very close to unit, meaning that any crystalline change during annealing is due to an increase in crystallite size and reduction of grain boundaries, as well as relaxation of the initial tensile stresses within the film.

Crystallite size of ZnO films has been estimated using the Scherrer formula. Fig. 2 illustrates the evolution of mean crystallite size (S) as a function of the sputtering power and annealing treatment. A steady decrease in crystallite size was noted upon increasing power but they tend towards a constant value after annealing treatment.

The sputtering power effect on crystallite size for the ZnO and AZO films was confirmed by AFM micrographs further depicted in Fig. 3. The surface morphology evolution for ZnO and AZO films was observed as a function of sputtering power before and after annealing treatment, at the same magnification order. From this figure, it can be seen that the obtained films are porous and while the crystallite size of as-prepared ZnO is slightly decreasing with sputtering power, after annealing treatment, it appears to be almost constant for all values. The AZO crystallite size is observed to be smaller than for the ZnO films obtained in the same conditions and it decreased with sputtering power. No cracks were observed upon annealing treatment for either ZnO or AZO films.

Further, the root-mean-square (RMS) roughness was measured. In Fig. 4, the effect of sputtering power on RMS roughness of ZnO and AZO films is depicted. For ZnO films, a small variation is observed in the values of the thin films before and after annealing. The RMS roughness appeared more stable upon annealing treatment and increasing the sputtering power above 110 W resulted in an increased roughness of ZnO films. In case of AZO films, the RMS roughness had a decreasing trend to a plateau of 1.9 nm. Increased sputtering power had an opposite effect on the AZO films resulting in lower roughness suggesting a conductivity improvement. As Oh showed, an increase

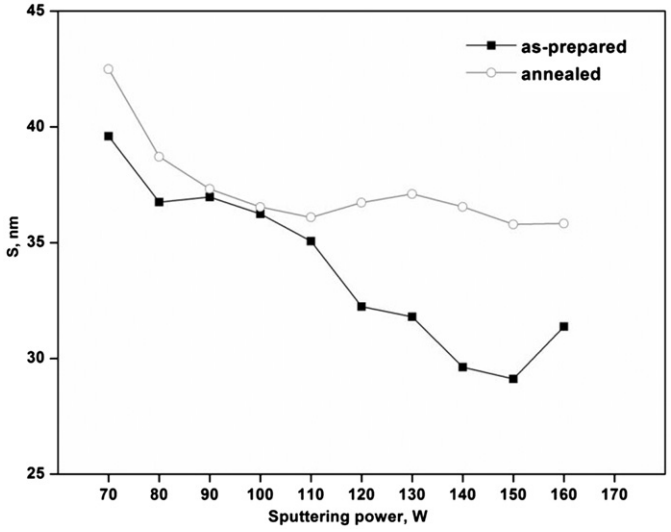

Fig. 2. Effect of the annealing treatment on the mean crystallite size for ZnO films.

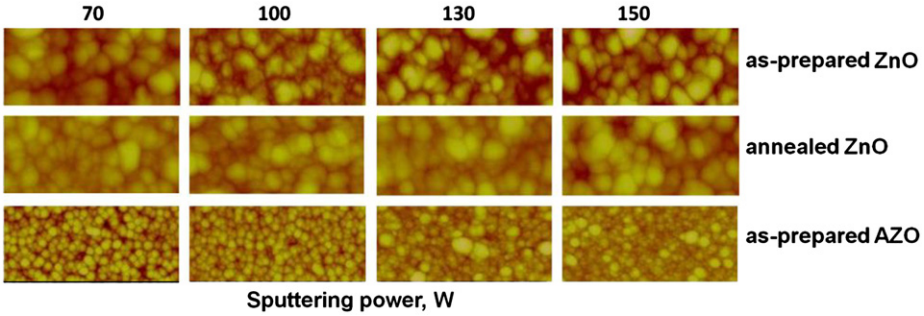

Fig. 3. AFM images of the ZnO and AZO films as a function of sputtering power and annealing treatment.

in roughness may cause deterioration of the electrical properties [25].

With regards to the deposition of AZO films, it was observed that films deposited at low pressures (<10 mTorr) exhibited the highest conductivities [13,26,27], although S. H. Jeong et al. found optimum conductivities when sputtering at approximately 30 mTorr [28]. However, sputtering is versatile. There is a high variety of systems different in sputtering configuration, geometry, target types etc. The orientation and placement of the substrate relative to the target can affect the deposition rate as well as the properties of obtained film [27]; moreover, the size of the sputtering target influences the power density. There are generally two modes of sputtering when considering the substrate exposition relative to the sputtering target; static and dynamic mode. During static mode both the substrate and sputtering target are stationary, whilst during dynamic mode the substrate is rotated [29]. This is done to prevent the known problem of the lateral change in the film properties [13]. It is assumed that the spatial variation in film properties is due to inhomogeneous distribution of oxygen at the substrate surface [30] or to the increased bombardment of the AZO films by energetic oxygen atoms of the substrate at the target erosion sites [29,30]. In this paper the films were sputtered by using static mode in order to have a better insight into the effect of sputtering conditions on the films properties. This approach was considered as an optimization step in the design of AZO film properties.

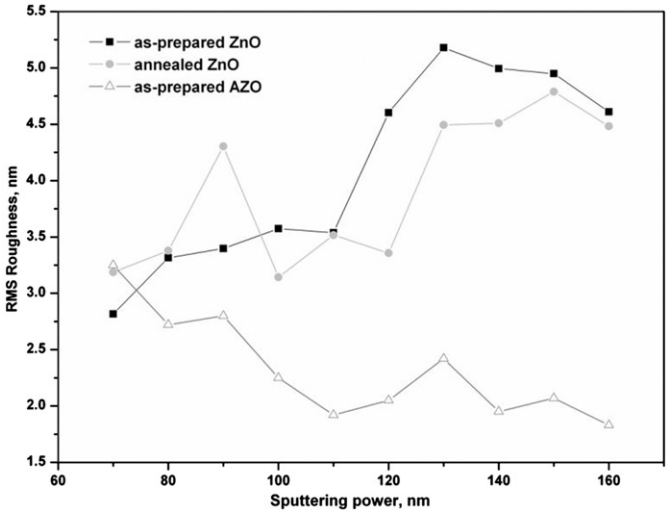

Fig. 4. RMS roughness evolution for ZnO and AZO films with the sputtering power, before and after annealing.

3.2. Optical properties

The curves in Fig. 5a and b summarize the optical transmittance (T) spectra as a function of wavelength (λ) in the visible spectrum for thin films of ZnO and AZO before and after annealing treatment. Overall, very high transmittance was noticed for all ZnO films ($>$ 85%) over the visible spectrum, considering 100% transmittance for the glass substrate. A very slight change of the optical transmittance of ZnO film as effect of annealing is shown in Fig. 5a. Before annealing, a marginal variation in the position of the transmittance curves with respect to the sputtering power is seen. These peaks shift after annealing treatments. These results are in good agreement with the XRD measurements as crystallite size varied with the sputtering power.

Fig. 5b displays the transmittance of the AZO films before and after the final annealing process at 600 °C. All AZO films displayed excellent optical properties, and as expected, an average transmittance, close to that of the ZnO ones. It was noted that AZO transmittance slightly increased upon annealing being related to a displacement of the absorption edge when thermal treatment was applied. The arrows in Fig. 5b show the redshift of the transmission for the as-prepared AZO films with increasing sputtering power.

The optical bandgaps were obtained from the transmittance spectra by plotting $(\alpha h\nu)^2$ vs. $h\nu$ (α is the absorption coefficient and $h\nu$ the photon energy) and extrapolating the straight line portion of this plot to the energy axis. These plots yielded bandgaps ranging 3.32–3.40 eV for AZO with respect to 3.31 eV for ZnO thin films. The increase of the bandgap of the AZO films indicates an increase in free charge carriers within the films, as explained by the Moss-Burstein effect [31]. A bandgap narrowing was observed with increasing sputtering power for the as-prepared films, as seen in Fig. 6. However, this relationship is non-existent for the annealed films.

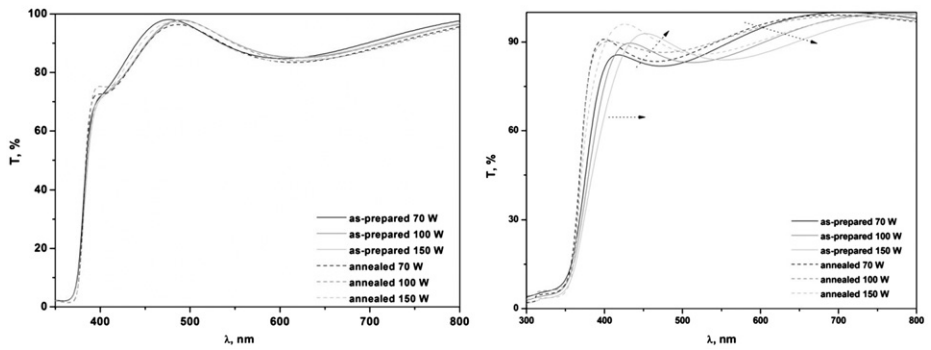

Fig. 5. The optical transmittance curves of (a) ZnO and (b) AZO films as a function of annealing treatment.

It is known that the bandgap of highly n-doped materials enlarges with increasing carrier concentration thanks to a blocking of the lowest states of the conduction band by excess electrons [32]. Therefore, in case of our thin films, the observed dependence of optical properties on the sputtering power before and after annealing treatment should be related to changes in the carrier concentration, considering a limit depending on the annealing atmosphere [24]. It was already reported that vacuum is effective in improving the carrier concentration, grain size and mobility of AZO films and that annealing can result in increase of bandgap energy [33].

3.3. Electrical properties

Further measurements were performed in order to relate the structural and electrical characteristics. As depicted in Fig. 7, the resistivity (ρ) of ZnO films didn't vary significantly upon annealing treatment. No change with the sputtering power was observed, either. Since the conductivity of ZnO is primarily due to oxygen vacancies and interstitial zinc ions [34], a decrease in conductivity is indicative of a fewer crystalline defects, and hence a reduction in the number of free charge carriers. In order to relate the fundamental electronic transport behavior to the dependence of resistivity, a scattering mechanism should be emphasized since the grain boundary plays an important role in determining the characteristic of carrier scattering for the un-doped polycrystalline ZnO film [35].

To study the annealing effects on the electronic properties of AZO, the films were annealed at 400, 500 and 600 °C. Four-point probe measurements of as-deposited films showed high resistance values for the AZO films in absence of annealing treatment as observed in Fig. 8A. Upon annealing at 400 °C, the resistivity (ρ) is reduced by several orders of magnitude and only a minimal change

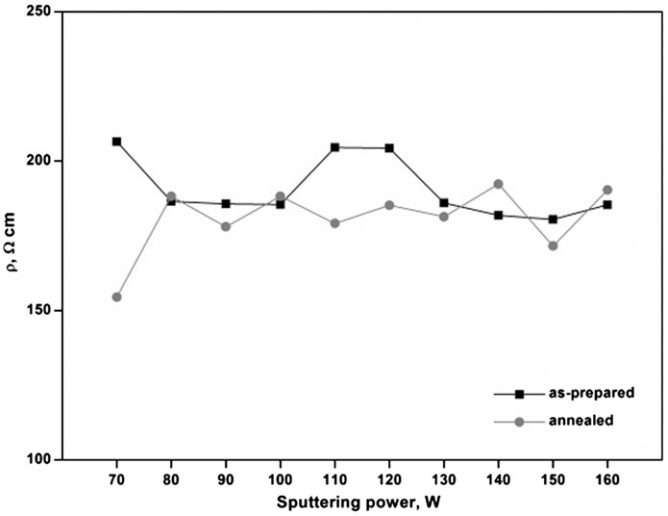

Fig. 7. Effect of annealing treatment on ZnO resistivity (ρ).

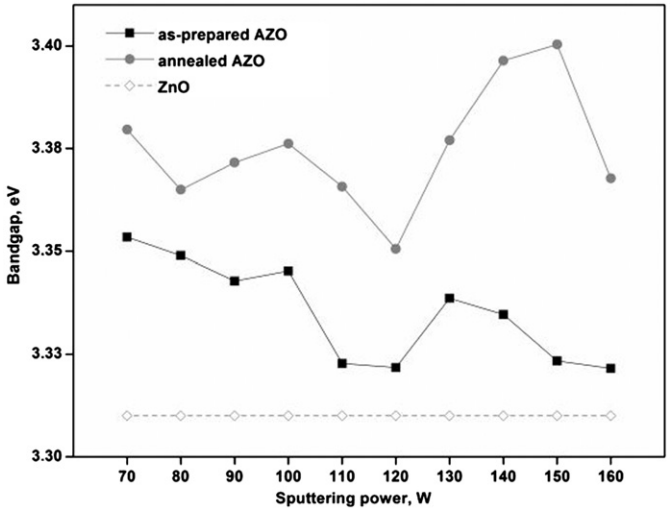

Fig. 6. Sputtering power dependence of ZnO and AZO bandgap energy (annealing treatment at 600 °C).

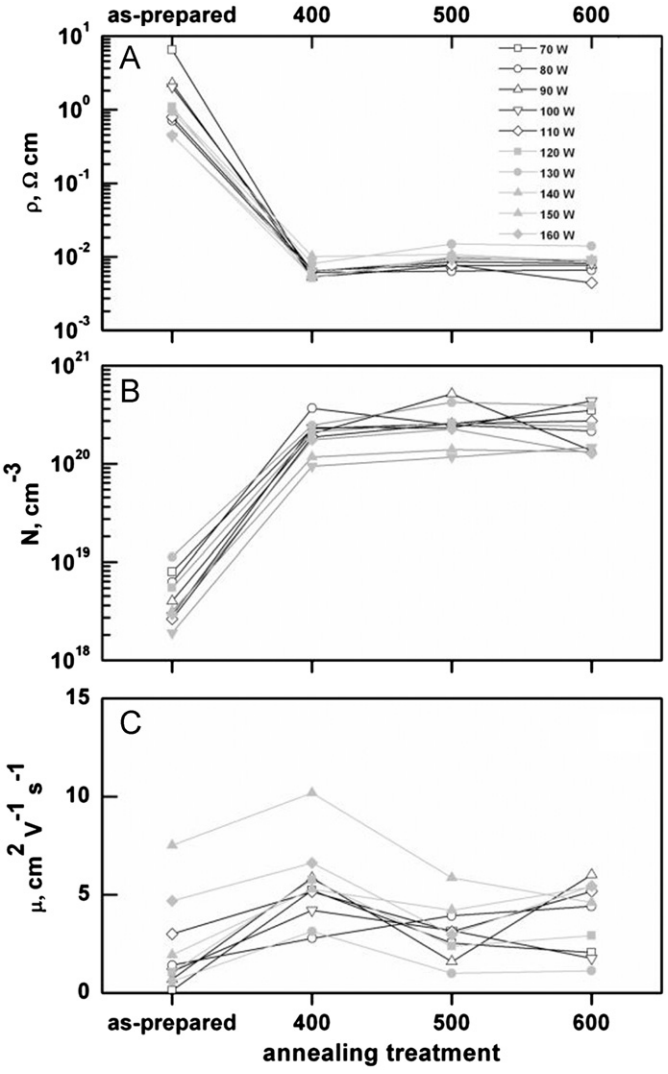

Fig. 8. Effects of annealing treatment on (A) resistivity (ρ); (B) carrier concentration (N) and (C) mobility (μ) of AZO films.

was seen with further increasing annealing temperature. The drop in resistivity upon annealing treatment could be attributed to the release of aluminum ions into the crystal lattice and expulsion of oxygen from the film [36]. It should be noted that the resistivity range narrowed for optimum annealing temperature achieved, indicating that the same electrical quality can be achieved with the various sputtering power. The origin of these resistivity changes has been investigated by determination of the carrier concentration and mobility for the different AZO films.

The Hall effect measurements showed a 20–100 fold increase in the carrier concentration (N) within the AZO films upon annealing treatment as observed in Fig. 8B. Generally, the films deposited at lower sputtering power exhibited higher carrier concentration values and as annealing temperature increased, the carrier concentration of AZO films showed a slight increase. It has been found that the carrier concentration tends to increase when the lattice distortion increases [37]. The changes in the carrier concentration of AZO films have also been related to creation or annihilation of donor oxygen vacancies [38], in addition to crystalline quality variations that modify the effective doping of Al onto Zn lattice sites [39].

An invariant trend of the carrier concentration as observed at higher sputtering values is indicative of degenerate semiconductors. As Zhang et al. showed, for the degenerate polycrystalline films with large crystallite size (much larger than mean free path of carriers) and high carrier concentration, ionized impurity scattering dominates the Hall mobility (μ) of the films and the Hall mobility is independent of temperature in low temperature range, while in high temperature range, thermal lattice vibration becomes the major scattering mechanism and the mobility is inversely proportional to temperature [40].

Generally, the mobility increased upon annealing treatment, showing the maximum value at 400 °C see Fig. 8C, regardless of sputtering power employed. The mobility as a function of annealing temperature exhibited a different behavior depending on the sputtering power and carrier concentration, respectively. The AZO films with the highest mobility were obtained at higher sputtering power values and showed a decrease of the mobility with increasing temperature. This decreasing trend of mobility as a function of annealing temperature became less evident with decreasing sputtering power. It can be concluded that the particle energies in the deposition process have a marked influence on the mobility values of AZO films, therefore both crystallinity and carrier concentration affect the mobility values [41]. The decrease of the mobility of our Ar-annealed AZO films could be attributed to a high grain boundary trap density that couldn't be overcome by the grain barrier scattering [42]. A significant change in mobility with respect to the carrier concentration due to the annealing processes is clearly evidenced in Fig. 9. The mobility improved over a factor of 10 with decreasing carrier concentration. Further attempts are needed to fully understand the carrier transport in AZO films.

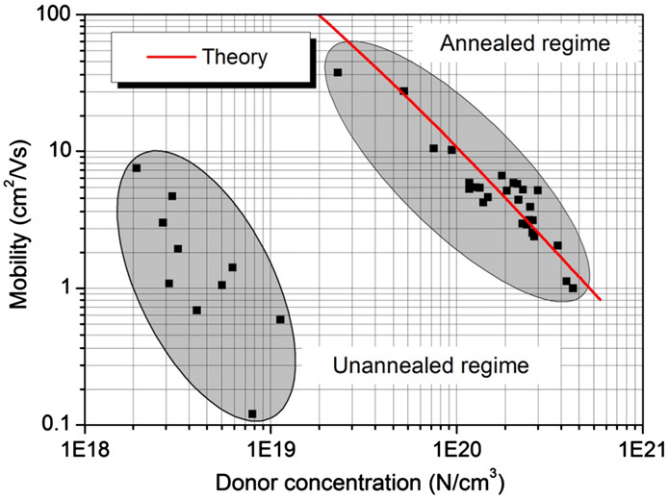

Fig. 9. Evolution of mobility (μ) with the carrier concentration (N) for the AZO films.

4. Conclusions

The ZnO and AZO thin film deposition parameters required for optimal electronic, structural and optical properties have been studied. Therefore, the results showed that increasing sputtering power induces modified crystallinity of the ZnO films and smaller crystallite sizes. AZO transmittance slightly increased upon annealing being related to a displacement of the absorption edge to the higher wavelengths when thermal treatment applied. The bandgap energies ranged 3.32–3.40 eV for AZO films and 3.31 eV for ZnO ones obtained in the same conditions. The resistivity of ZnO films didn't present significant changes with varying parameters, while AZO resistivity was reduced by several orders of magnitude upon annealing at 400 °C. Generally, the films deposited at lower sputtering power exhibited higher carrier concentration values and moreover, as annealing temperature increased, the carrier concentration of AZO films showed a slight increase indicating crystalline quality variations that modify the effective doping of Al onto Zn lattice sites and probable lattice distortion. The mobility of AZO films increased upon annealing treatment, showing the maximum value at 400 °C, regardless of sputtering power employed. The AZO films with the highest mobility were obtained at higher sputtering power values and showed a decrease of the mobility with increasing annealing temperature. This suggests a strong influence of particle energies in the deposition process and the decreasing trend could be attributed to a high grain boundary trap density.

Acknowledgments

This work was partly funded by the Research Directorate of the European Commission by the Integrated project IFOX under the contract no. 246102. The authors also thank the Center for Space Human Robotics of Italian Institute of

Technology (IIT) of Turin (Italy) for the support provided on the electron mobility characterization.

References

[1] F. Padinger, R. Rittberger, N. Sariciftci, Advanced Functional Materials 13 (2003) 85–88.
[2] Y.C. Lin, S.J. Chang, Y.K. Su, T.Y. Tsai, C.S. Chang, S.C. Shei, C.W. Kuo, S.C. Chen, Solid-State Electron 47 (2003) 849–853.
[3] J.S. Kim, M. Granström, R.H. Friend, N. Johansson, W.R. Salaneck, R. Daik, W.J. Feast, F. Cacialli, Journal of Applied Physics 84 (1998) 6859–6870.
[4] K. Wasa, S. Hayakawa, T. Hada, Japanese Journal of Applied Physics 10 (1971) 1732-1732.
[5] D. Pullini, A. Pruna, S. Zanin, D. Busquets, Journal of Electrochemical Society 159 (2012) E45–E51.
[6] A. Pruna, D. Pullini, D. Busquets Mataix, Journal of Electrochemical Society 159 (2012) E92–E98.
[7] W. Jeong, G. Park, Solar Energy Materials and Solar Cells 65 (2001) 37–45.
[8] B.E. Sernelius, K.F. Berggren, Z.C. Jin, I. Hamberg, C.G. Granqvist, Physical Review B 37 (1988) 10244–10248.
[9] A. Suresh, P. Wellenius, A. Dhawan, J. Muth, Applied Physics Letters 90 (2007) 123512.
[10] Y.S. Jung, J.Y. Seo, D.W. Lee, D.Y. Jeon, Thin Solid Films 445 (2003) 63–71.
[11] J. Rousset, E. Saucedo, D. Lincot, Chemistry of Materials 21 (2009) 534–640.
[12] I.M. Ritchie, R.K. Tandon, Surface Science 22 (1970) 199–215.
[13] S. Calnan, J. Hüpkes, B. Rech, H. Siekmann, A.N. Tiwaria, Thin Solid Films 516 (2008) 1242–1248.
[14] B.S. Chua, S. Xu, Y.P. Ren, Q.J. Cheng, K. Ostrikov, The Journal of Alloys and Compounds 485 (2009) 379–384.
[15] T. Minami, Thin Solid Films 516 (2008) 5822–5828.
[16] J.F. Chang, H.H. Kuo, I.C. Leu, M.H. Hon, Sensors Actuators B 84 (2002) 258–264.
[17] N. Chantarat, S.H. Hsu, C.C. Lin, M.C. Chiang, S.Y. Chen, Journal of Materials Chemistry 22 (2012) 8005–8012.
[18] W.T. Yen, J.H. Ke, H.J. Wang, Y.C. Lin, J.L. Chiang, Advanced Materials Research 79-82 (2009) 923–926.
[19] H.Y. Shin, M.H. Joo, S.K. Moon, T.H. Moon, K.H. Park, Surface and Interface Analysis (2012)http://dx.doi.org/10.1002/sia.4967.
[20] A.F. Aktaruzzaman, G.L. Sharma, L.K. Malhotra, Thin Solid Films 198 (1991) 67–74.
[21] Y.-C. Liang, Ceramics International 38 (2012) 119–124.
[22] S. Lee, Y. Kim, H. Shin, J. Song, Journal of the Korean Physical Society 53 (2008) 188–191.
[23] K. Ellmer, Journal of Physics D: Applied Physics 33 (2000) R17–R32.
[24] S.S. Lin, J.L. Huang, P. Sajgalik, Surface and Coatings Technology 185 (2004) 254–263.
[25] B.Y. Oh, M.C. Jeong, D.S. Kim, W. Lee, J.M. Myoung, Journal of Crystal Growth 281 (2005) 475–480.
[26] X. Hao, J. Ma, D. Zhang, T. Yang, H. Ma, Y. Yang, C. Cheng, J. Huang, Applied Surface Science 183 (2001) 137–142.
[27] M.K. Jayaraj, A. Antony, M. Ramachandran, Bulletin on Material Science 25 (2002) 227–230.
[28] S.H. Jeong, J.W. Lee, S.B. Lee, J.H. Boo, Thin Solid Films 435 (2003) 78–82.
[29] R.J. Hong, X. Jiang, B. Szyszka, V. Sittinger, S.H. Xu, W. Werner, G. Heide, Journal of Crystal Growth 253 (2003) 117–128.
[30] K. Tominga, K. Kuroda, O. Tada, Japanese Journal of Applied Physics 27 (1988) 1176–1180.
[31] E. Burstein, Physical Review 93 (1954) 632–633.
[32] M. Suchea, S. Christoulakis, N. Katsarakis, T. Kitsopoulos, G. Kiriakidis, Thin Solid Films 515 (2007) 6562–6566.
[33] G.J. Fang, D. Li, B.L. Yao, Thin Solid Films 418 (2002) 156–162.
[34] T.E. Murphy, D.Y. Chen, J.D. Phillips, The Journal of Electronic Materials 34 (2005) 699–703.
[35] F.R. Blom, F.C.M. Van de Pol, G. Bauhuis, Th.J.A. Popma, Thin Solid Films 204 (1991) 365–376.
[36] J.J. Ding, H.X. Chen, S.Y. Ma, Applied Surface Science 256 (2010) 4304–4309.
[37] C. Guillén, J. Herrero, Vacuum 84 (2010) 924–929.
[38] M. Bouderbala, S. Hamzaoui, M. Adnane, T. Sahraoui, M. Zerdali, Thin Solid Films 517 (2009) 1572–1576.
[39] A.M.K. Dagamseh, B. Vet, F.D. Tichelaar, P. Sutta, M. Zeman, Thin Solid Films 516 (2008) 7844–7850.
[40] D.H. Zhang, T.L. Yang, Q.P. Wang, D.J. Zhang, Materials Chemistry and Physics 68 (2001) 233–238.
[41] T. Minami, Semiconductor Science and Technology 20 (2005) S35–S44.
[42] K. Ellmer, R. Mientus, Thin Solid Films 516 (2008) 4620–4627.